Geophysical Research Letters

RESEARCH LETTER
10.1029/2023GL104784

Anthropogenic Weakening of the Atmospheric Circulation During the Satellite Era

Sisam Shrestha[1] **and Brian J. Soden**[1]

[1]Rosenstiel School of Marine, Atmospheric, and Earth Science, University of Miami, Coral Gables, FL, USA

Key Points:

- The global atmospheric overturning circulation has weakened in recent decades despite a strengthening of the Walker Circulation
- Climate models predict a circulation weakening consistent with observations, manifested primarily as a weakening of the zonally asymmetric overturning circulation
- The observed weakening is reproduced in coupled climate models only when anthropogenic forcing is included

Supporting Information:

Supporting Information may be found in the online version of this article.

Correspondence to:

S. Shrestha,
sisam.shrestha@earth.miami.edu

Citation:

Shrestha, S., & Soden, B. J. (2023). Anthropogenic weakening of the atmospheric circulation during the satellite era. *Geophysical Research Letters*, *50*, e2023GL104784. https://doi.org/10.1029/2023GL104784

Received 5 JUN 2023
Accepted 3 NOV 2023

Abstract Climate models predict a slowing of the atmospheric overturning circulation with warming. In models, this slowing manifests primarily as a weakening of the Walker Circulation (WC). However, observational studies indicate a strengthened Pacific WC over the past several decades, raising questions about the models' ability to represent critical energetic and hydrologic constraints responsible for the predicted weakening. This discrepancy is closely tied to differences in the warming pattern over the Pacific during this period. We show that model simulations with either observed or model-projected warming patterns predict a robust weakening of atmospheric overturning circulation, despite having opposing changes in the Pacific WC strength. This weakening occurs in the zonally asymmetric circulation, rather than in the zonal-mean Hadley cell. Weakening inferred from satellite observations is reproduced in coupled models only when anthropogenic forcing is included, suggesting that a human-induced weakening of the global atmospheric circulation is already detectable in observations.

Plain Language Summary The atmospheric circulation transfers moisture and energy from the tropics to the polar regions and regulates the distribution of rainfall in the tropics which is home to around 40% of the world's population. In recent years, observations show a strengthening of the Pacific Walker Circulation (WC), a regional-level circulation, which contrasts the weakening of the circulation predicted by climate models. This discrepancy questions the climate models' ability to predict future changes in overturning circulations. Using various strength indices, we find a consistent "weakening with warming" of the global overturning circulation in both observations and climate models for the common period, regardless of the behavior of regional-level circulations. Moreover, we find that it is highly unlikely that this observed weakening is due to natural variations in the climate.

1. Introduction

Changes in the hydrological cycle in response to a warming climate provide a constraint on the atmospheric overturning circulation that can be understood in terms of differences in the rate of increase between precipitation and boundary-layer moisture (Held & Soden, 2006). Because precipitation increases more slowly (~2%/K) than the mixing ratio of water vapor in the boundary layer (~7%/K), this necessitates a reduction in the overturning of mass in the troposphere as the climate warms, that is, the convective mass flux (M_c) must decrease. Our confidence in these differing rates of change is high as they are grounded in basic thermodynamic and energetic arguments; water vapor increases being governed by the Clausius-Clapeyron relation and precipitation increases being regulated by changes in atmospheric radiative cooling (Allan et al., 2022; Held & Soden, 2006; Lambert & Webb, 2008). Similar constraints can be inferred from the increase in dry static stability compared to radiative cooling of the troposphere (Knutson & Manabe, 1995; O'Gorman & Singh, 2013). Indeed, evidence of the fundamental nature of these constraints is found in the commonality of model responses to anthropogenic forcing—all the coupled ocean-atmosphere models project a weakening of the atmospheric circulation in response to warming (Bony et al., 2013; Chadwick et al., 2013; Ma et al., 2012; Power & Smith, 2007; Vecchi & Soden, 2007).

Weakening of the global atmospheric circulation is not uniform. In coupled models, it primarily manifests as a weakening of the zonally asymmetric component of the overturning circulation or, more specifically, the Pacific Walker Circulation (WC) (Held & Soden, 2006; Vecchi & Soden, 2007). However, studies using observations suggest a weakening of the Pacific WC over much of the 20th century, followed by a strengthening during the past several decades despite substantial warming (Bellomo & Clement, 2015; Chung et al., 2019; DiNezio et al., 2013; Kociuba & Power, 2015; L'Heureux et al., 2013; McGregor et al., 2014; Meng et al., 2012; Power & Kociuba, 2011; Sandeep et al., 2014; Sohn et al., 2013; Tokinaga et al., 2012; Vecchi et al., 2006; Wu

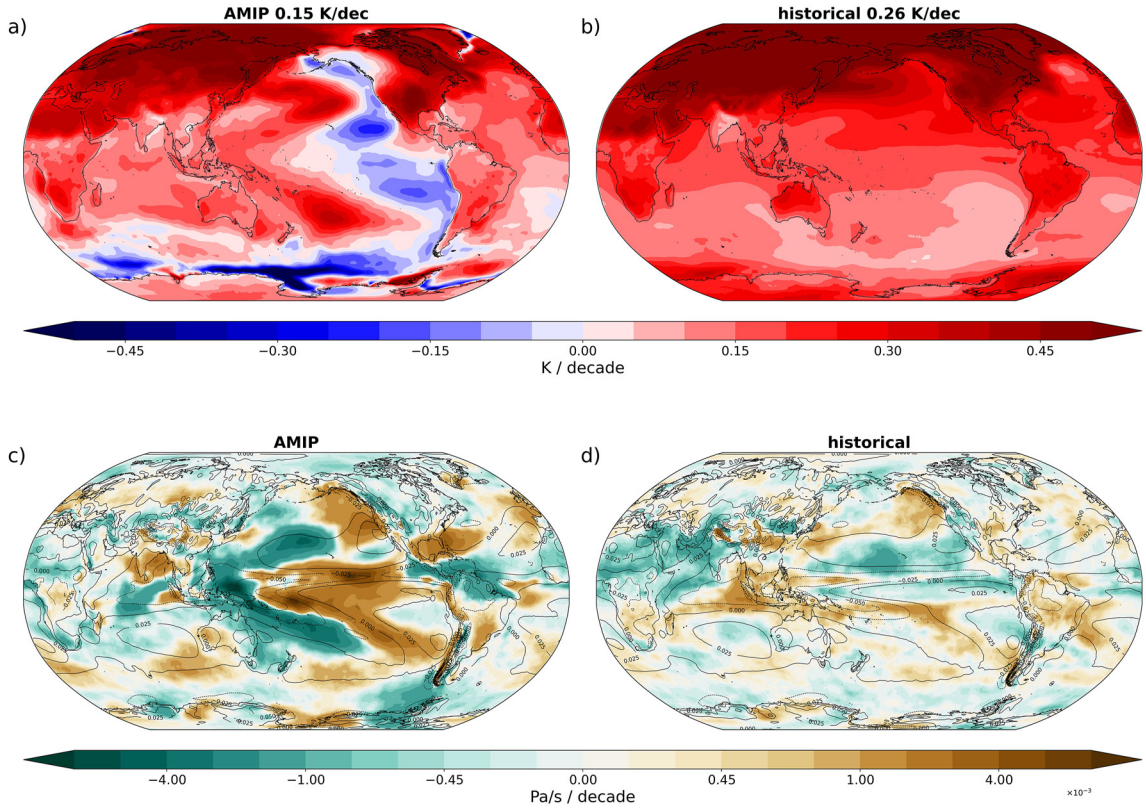

Figure 1. *Differing sea surface temperature and ω_{500} patterns between CMIP6 AMIP and coupled historical experiments*: multi-model mean decadal trend (1979–2014) in surface air temperature (a, b) and mid-tropospheric vertical pressure velocity, ω_{500} (c, d) for AMIP (left) and historical (right) simulations from CMIP6. Decadal trend for the global-mean surface air temperature is reported on top of each plot.

et al., 2021). At a millennium scale, paleo-proxy reconstructions show insignificant shift in long-term Pacific WC trend between the pre- and post-industrial onset era (Falster et al., 2023).

The Pacific WC strength is closely tied to the east-west sea surface temperature (SST) gradient over the equatorial Pacific (Sandeep et al., 2014). Observed SST trends over recent decades indicate warming in the western Pacific and cooling in the eastern Pacific, enhancing the east-west SST gradient (Figure 1a and Figure S1 in Supporting Information S1). However, coupled climate models forced with observed changes in greenhouse gases project a reduction in the east-west SST gradient as response to historical radiative forcings (Figure 1b and Figure S1 in Supporting Information S1). These contrasting patterns of surface warming drive contrasting responses of the atmospheric circulation; coupled ocean-atmosphere models simulate a weakening of the Pacific WC over this period, while observations indicate a strengthening (Figure S2 in Supporting Information S1). This robust discrepancy between the coupled model simulations and the observed trends thus reflects either a fundamental problem in model projection to the forced response or a systematic underestimate in their simulation of the Pacific decadal variability (Lee et al., 2022).

Early attempts to reconcile this discrepancy pointed to internal variability on decadal time scales as a potential explanation (Chung et al., 2019; Power et al., 2021; Watanabe et al., 2021; Wu et al., 2021). This would imply that the strengthening of the Pacific WC in recent decades reflects the appearance of low-frequency modes of natural variability, such as the Interdecadal Pacific Oscillation (IPO) or Atlantic Multidecadal Oscillation (Bordbar et al., 2017; Murphy et al., 2017).

However, as the divergence between observed and model-projected trends has persisted, this explanation has become increasingly unlikely (Seager et al., 2022; Wills et al., 2022). Strengthened Pacific trade winds during the early 2000s global warming hiatus was stronger than that associated with a negative IPO phase and outside the range of model simulations (England et al., 2014). Recent studies that examine large ensembles of model simulations indicate that the persistence of observed warming pattern over the Pacific lies at the extreme limit of

model behavior and is therefore unlikely to result from internal variability (Seager et al., 2022). This would imply that the observed trends in SST and the Pacific WC are actually a forced response to increasing greenhouse gases. However, due to their coupled nature, it's unclear if a strengthened Pacific WC drives the asymmetric pattern of SST change, or vice-versa. This, in turn, raises questions about the validity of model projections of a weakened atmospheric circulation.

Changes in the atmospheric overturning circulation have important implications for the pattern of precipitation change, as well as the frequency of droughts and extreme precipitation events (Chadwick et al., 2013; Lau & Kim, 2015; Su et al., 2014, 2019; Wodzicki & Rapp, 2020). Atmospheric overturning circulation and SST pattern are closely tied to the climate feedback from tropical low cloud covers and thus has a strong impact on climate sensitivity (Andrews et al., 2022; Loeb et al., 2020; Sherwood et al., 2014). Understanding how atmospheric overturning circulations have behaved in recent decades is thus imperative to predict their evolution under future conditions and to formulate mitigation and adaptation policies related to climate change.

2. Data and Methods

2.1. Strength Indices for Large-Scale Atmospheric Circulation

We employed three different estimates to quantify the strength of atmospheric overturning circulations. The first index used is the change in the convective mass flux (ΔM_c) which is also the preferred value to detect changes in atmospheric circulation as it is a direct measure of convection. In a warming world, the differential rate of increase between boundary-layer moisture and precipitation requires a weakening of large-scale atmospheric circulations at a rate of ∼5%/K (Held & Soden, 2006). However, most CMIP6 models used in this study have not archived their convective mass flux output. Following Held and Soden (2006), we estimated convective mass flux as

$$\Delta M_c^* = \Delta P/P - \Delta q/q, \tag{1}$$

where P is the precipitation and q is the boundary-layer specific humidity. For models that archived the convective mass flux, ΔM_c^* agrees well with the model-simulated ΔM_c at 500 hPa (Figure S3 in Supporting Information S1). We find similar results for the vertically integrated ΔM_c (surface to 30 hPa) since the vertical profiles of convective mass flux don't show a significant change during this period.

The second index used is the fractional change in the upward component of the mid-tropospheric vertical pressure velocity ($\omega_{500}{}^{+}$) (Bony et al., 2013; Vecchi & Soden, 2007). As the circulation weakens, following the simple mass-balance theory, tropical-mean $\omega_{500}{}^{+}$ is also expected to weaken (Vecchi & Soden, 2007). We used a daily ω_{500} data set to construct a monthly data set of only $\omega_{500}{}^{+}$.

The third index we employed is the change in the spatial variance for ω_{500} which should decrease at twice the rate of the mean, provided the weakening of the vertical velocity is proportional to the preexisting vertical velocity field (Held & Soden, 2006). The spatial variance index can further be separated into a component related to the zonal-mean circulation, for example, Hadley circulation, and the zonally asymmetric circulation, like the WC. Since changes in the atmospheric circulation are expected to manifest in both ascent and descent regions (Su et al., 2014), we consider changes in the spatial variance of ω_{500} instead of just $\omega_{500}{}^{+}$ as in previous studies (Held & Soden, 2006; Vecchi & Soden, 2007).

Time series were deseasonalized using a base period of 1990–2010. Fractional changes are computed with reference to the first 10 years of the time series. We define the tropics as the region bound by the 30° latitude band. Trends were computed using least squares linear regression. A negative trend in the timeseries implies a weakening of the circulation. Uncertainty was calculated using a two-sided Student's t-test, considering the autocorrelation of noise in a time series (Weatherhead et al., 1998), and can be understood as a reflection of the interannual variability. Observed trends are reported with ±2 Standard Errors (SE) and can be considered significant at the 95% confidence interval if it is greater than ±2 SE.

2.2. Climate Models

To analyze changes in recent decades, we employed 25 coupled ocean-atmosphere models forced with historical radiative forcings (1850–2014) from the Coupled Model Intercomparison Project Phase 6 (CMIP6, Eyring

et al., 2016) along with the corresponding atmosphere-only simulations integrated using observed SSTs as a lower boundary condition from the Atmospheric Model Intercomparison Project (AMIP, Gates et al., 1999) (1979–2014) (Table S1 in Supporting Information S1). To analyze the contribution of anthropogenic forcings on the observed trends in atmospheric overturning circulation, we extended the coupled historical experiments to 2021 using the ssp5-8.5 ScenarioMIP (O'Neill et al., 2016), which represents a high-emission future pathway that produces a radiative forcing of 8.5 W m^{-2} in 2100. We also used 90 members from the CESM2 Large Ensemble Project (CESM2-LENS; Rodgers et al., 2021) and the 10-member Community Atmosphere Model version 6 prescribed SST Global AMIP (CAM6 AMIP) (Danabasoglu et al., 2020) ensemble that extends the prescribed SST AMIP experiments to 2021. To analyze the contribution of unforced climate variability on the observed trend, we used preindustrial control (piControl) experiment that is representative of conditions before the onset of large-scale industrialization in 1850. We only used the first ensemble member (r1i1p1f1) from each model, except for the large ensembles, to ensure all the models are weighted equally in the multi-model mean (MMM) calculation.

2.3. Observations

For the estimation of changes in the observed atmospheric overturning circulation, we used precipitation observations from Global Precipitation Climatology Project v2.3 (GPCP v2.3, Adler et al., 2003) which combines precipitation from satellites, rain gauges and soundings to provide a global rainfall record. GPCP data before 1988 is, however, limited to IR-based estimates. The monthly data set runs from 1979 to the present day and is provided in a 2.5° × 2.5° grid. For boundary-layer moisture, we used total precipitable water (TPW) from the Merged Precipitable Water 1° Monthly Climate Product from Remote Sensing Systems (Remote Sensing Systems, 2016). The TPW data set has been constructed using intercalibrated microwave radiometers that provide data from 1988 to the present day over global ice-free oceans. We used European Centre for Medium-Range Weather Forecasts v5 reanalysis (ERA5) data set (Hersbach et al., 2023) to fill in the data gaps and construct a global TPW data set. Both the TPW data sets have a similar interannual trend over ice-free oceans for the common period (1988–2021) (Figure S4 in Supporting Information S1; Allan et al., 2022). TPW provides a good estimate of the near-surface specific humidity since much of the atmospheric water content is concentrated in the boundary layer, as seen from the strong positive correlation between the fractional changes in near-surface specific humidity and TPW (Figure S5 in Supporting Information S1). However, since TPW is a column integral, it tends to overestimate the change in boundary-layer specific humidity (and thus ΔM_c) with warming since the fractional increase in saturation vapor pressure is inversely proportional to temperature, that is, $d\ln(e_s)/dT \sim 1/T^2$. Thus, we use a linear regression between monthly anomalies in near-surface specific humidity and TPW from the AMIP MMM to derive an observational estimate for near-surface specific humidity (Figure S5 in Supporting Information S1). We used NASA GISS Surface Temperature Analysis version 4 (GISTEMP v4) to estimate global surface temperature change (GISTEMP Team, 2023; Lenssen et al., 2019).

3. Results

3.1. Model Projections of Pacific Warming and Large-Scale Atmospheric Circulation Change

Difference in the SST trend patterns between the coupled and the AMIP simulations is reflected in their respective ω_{500} trends (Figures 1c and 1d). The AMIP models simulate an increased ascending motion in the western Pacific and an increased subsidence in the eastern Pacific, consistent with a strengthened Pacific WC. This increase in the equatorial Pacific ω_{500} gradient is consistent with observations of SLP, water vapor transports and reanalysis data sets (Chung et al., 2019; Sohn & Park, 2010). In contrast, the CMIP6 coupled models simulate an opposing pattern, that is, a weakening of the equatorial Pacific ω_{500} gradient, reflecting a weakened Pacific WC.

To investigate the role of SST patterns on the atmospheric overturning circulation, we analyze trends in three different indices used to quantify the strength of the global-mean atmospheric circulation. For brevity, we focus on the ΔM_c^* index here, but similar results are found for the other two strength indices (Figure S6 in Supporting Information S1). For the coupled historical experiments, all three indices indicate a weakening of the atmospheric overturning circulation over the 1979–2014 period (Figure 2 right), consistent with the expected "weakening with warming" mechanism. Despite a large intermodel spread in the historical ensemble (attributable to the different interannual variability amongst models), all the members capture the temporary cooling associated with the

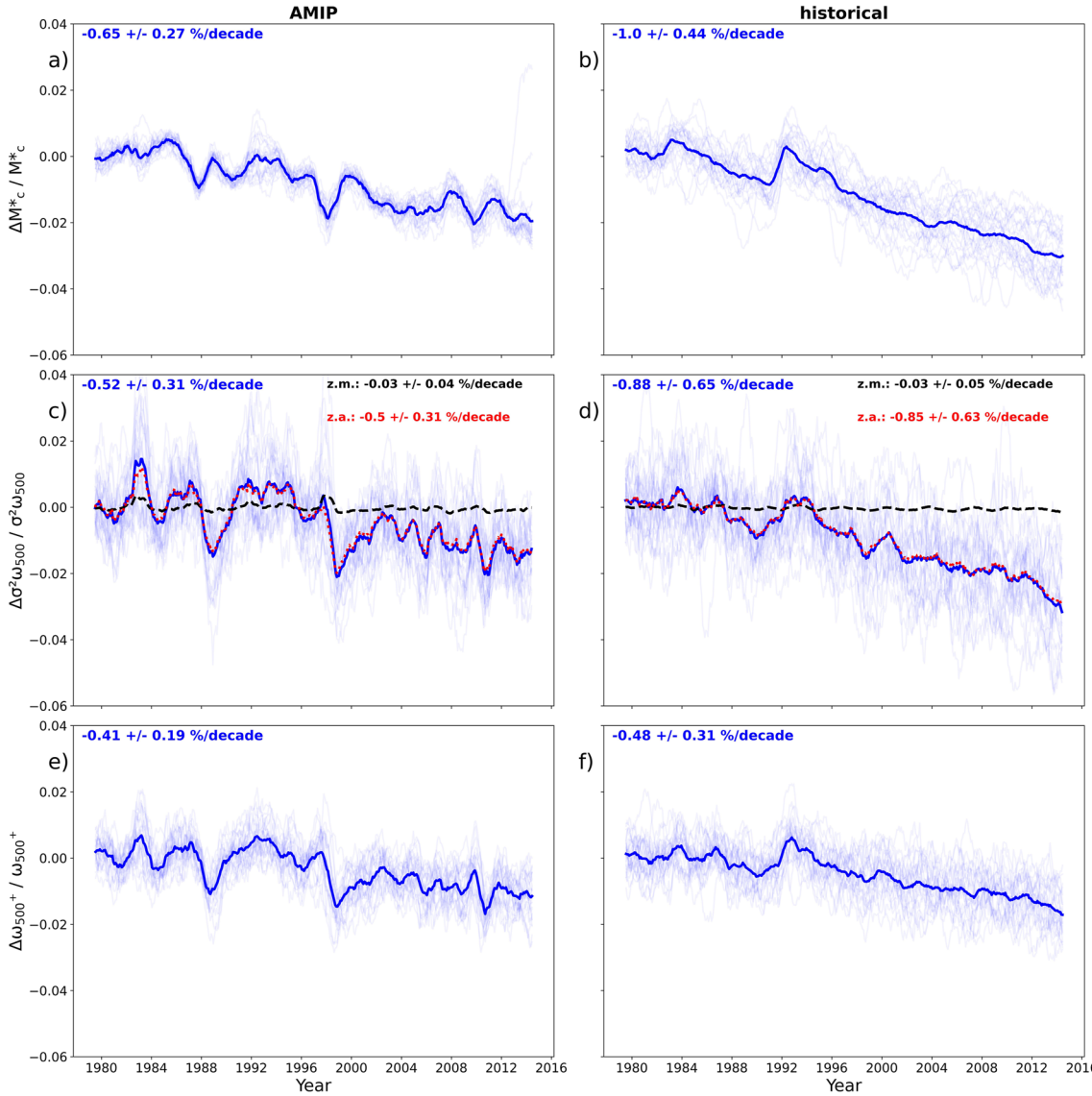

Figure 2. *Weakening of large-scale atmospheric circulation in CMIP6 experiments*: Global-mean fractional change in the convective mass flux (a, b), the spatial variance in ω_{500} (c, d) and the upward component of ω_{500} (e, f) for AMIP (left) and coupled historical (right) simulations. Multi-model mean (MMM) is denoted by the thick blue line. Decadal trend for MMM along with the intermodel spread ($\pm 2\sigma$) is shown in blue insets for each plot. Changes in the total spatial variance in ω_{500} are further decomposed into changes in the zonal-mean variance (black dashed) and zonally asymmetric variance (red dotted). Individual time series are smoothed using a 13-month running average.

aerosols released into the stratosphere following the Mt. Pinatubo eruption in 1991. This period of cooling corresponds with a brief strengthening of the atmospheric overturning circulation in all the models.

Although the AMIP simulations markedly differ from the coupled historical experiments in terms of the pattern of circulation response (Figure 1c), all models simulate a weakening atmospheric overturning circulation for this period (Figure 2 left). The AMIP MMM weakening falls within the historical intermodel spread, however, the magnitude of weakening is smaller for the AMIP experiments, in part due to the smaller global-mean temperature change in AMIP compared to the coupled model simulations. The MMM time series shows interannual variations associated with ENSO. Short-term weakening (strengthening) of global-mean circulation corresponds with warming (cooling) associated with major El Niño (La Niña) events like 1982–1983 and 1997–1998 (1988–1989 and 2000).

Changes in $\omega_{500}{}^{+}$ index and the spatial variance of ω_{500} also indicate a weakening of the global-mean atmospheric circulation for this period in both the simulations. Changes in the spatial variance of ω_{500} are dominated by the

weakening of the zonally asymmetric component of the circulation for both experiments (Figures 2c and 2d). The result that models preferentially weaken the asymmetric circulation rather than the zonal-mean circulation was first pointed out by Held and Soden (2006) and Vecchi and Soden (2007). Although not demonstrated, the possible explanation given by those studies was that zonal-mean circulation is constrained by momentum and meridional energy transport constraints, whereas the zonally asymmetric circulation is not. Thus, despite different warming patterns and contrasting responses of the Pacific WC, both the atmosphere-only and coupled historical experiments simulate a weakening of the global-mean atmospheric circulation, almost exclusively by a reduction in the zonally asymmetric component of the overturning circulation rather than the zonal-mean. In the coupled historical experiments, this weakening of the zonally asymmetric overturning circulation primarily manifests as a reduction in the Pacific WC. However, in the AMIP simulations, the weakening of the zonally asymmetric circulation occurs despite a strengthening of the Pacific WC. Thus, it is not necessary for the Pacific WC to weaken in order for models to simulate a weakening of the zonally asymmetric overturning circulation; other modes of the zonally asymmetric circulations (e.g., monsoons) are presumably responsible for this weakening.

3.2. Changes Inferred From Observations

Due to the lack of a global observational record for $\omega_{500,}$ we quantify observed changes in atmospheric overturning circulation using satellite measurements of precipitation and water vapor to compute ΔM_c^* following the same approach used for the models. The observation analysis begins in 1988 when microwave satellite measurements of TPW and precipitation first became available.

Consistent with the model simulations, observations also indicate a weakening of the global-mean atmospheric circulation. The magnitude of weakening (-0.51 ± 0.3%/decade) is comparable to the AMIP MMM weakening (-0.65 ± 0.37%/decade) but noticeably smaller than the weakening projected in the MMM of the coupled model simulations (-1.11 ± 0.51%/decade) for the 1988–2014 period. This discrepancy arises partly from the different rates of warming between observations and coupled model simulations. To account for the different warming rates, we compute the change in convective mass flux per unit temperature change, by dividing the trends in convective mass flux by trends in global-mean surface air temperature. The normalized changes in convective mass flux are comparable between the observed (-3.02%/K), AMIP (-4.64 ± 2.64%/K), and coupled model (-3.7 ± 0.83%/K) simulations. The larger spread in the AMIP is mainly due to an outlier, FGOALS-g3 which has a near-zero global-mean temperature trend and simulates a large weakening of the global overturning circulation (~ -10%/K) and an unusually large strengthening of the tropical overturning circulation (~ 25%/K). Removing the FGOALS-g3 model results in an AMIP weakening of -4.58 ± 1.13%/K.

To better understand the contributions of anthropogenic forcing to the observed trend in ΔM_c, we extend the historical coupled simulations to 2021 using the ssp5-8.5 ScenarioMIP. Using an alternative ScenarioMIP to extend the data set does not produce a significantly different result, as the ScenarioMIPs do not diverge significantly during the first few years. The extended observational record indicates a robust weakening of both the global- (-0.95 ± 0.21%/decade) and the tropical-mean (-0.63 ± 0.28%/decade) ΔM_c^* (Figure 3).

Compared to the CMIP6 ensemble, where differing model physics contributes to the ensemble spread, large ensembles like CESM2-LENS have the advantage of sharing the same model physics. Thus, the CESM2-LENS average and spread can be considered as the forced response and internal variability, respectively. Despite their different phases of internal variability, all the CESM2-LENS members exhibit a robust weakening of the atmospheric overturning circulation (Figure 3). While the CESM2-LENS spread captures the observational estimate of the weakening, the ensemble-mean weakening is stronger than the observational estimate (Figure S7 in Supporting Information S1), which may reflect the higher sensitivity of CESM2-LENS ensemble average (Figure 4). The historical MMM has a similar magnitude of weakening for both the 1988–2021 and 1979–2014 period (blue and pale blue lines, Figure 4).

The 10-member CAM6 AMIP ensemble also shows a robust weakening of the atmospheric overturning circulation (Figure 3). The magnitude of weakening for the CAM6 AMIP average is comparable to the observed global-mean weakening, highlighting the robustness of the weakening signal of atmospheric circulations in recent decades (Figure S7 in Supporting Information S1). The observed tropical-mean weakening, however, lies on the extreme of simulated trends, suggesting models' inability to simulate observed weakening in the tropics. We find a correlation of 0.7 and 0.4 between the observational estimate and CAM6 AMIP average for global and tropical convective mass flux change, respectively. The lower correlation in the tropics (also present for the shorter AMIP

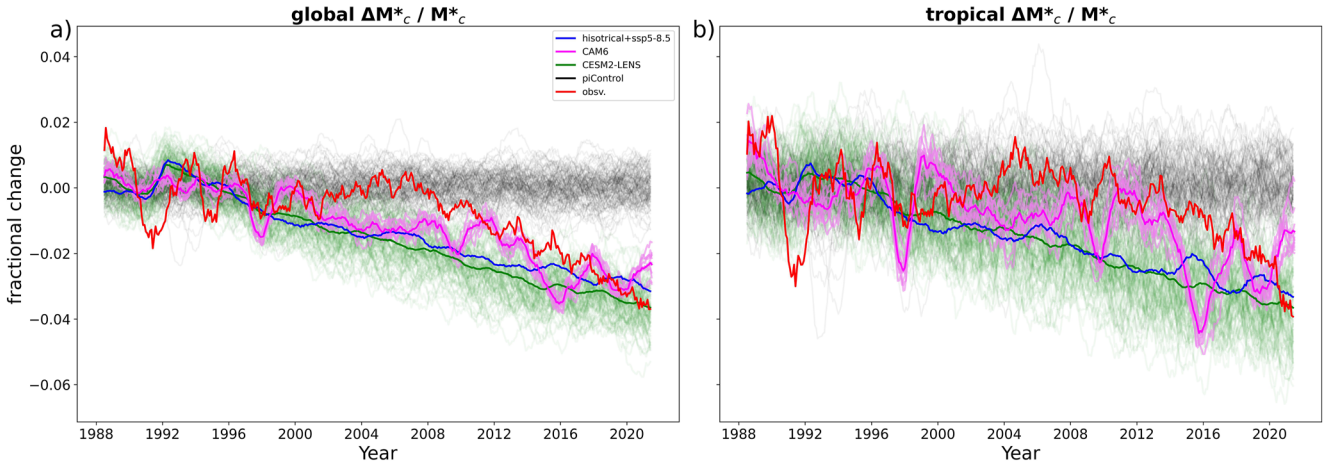

Figure 3. *Implications of internal variability on the weakening of large-scale atmospheric circulation*: Time series of fractional change in (a) global- and (b) tropical-mean convective mass flux for the ensemble mean of CESM2-LENS historical (green), CAM6 AMIP ensemble (pink), CMIP6 coupled historical + ssp5-8.5 (blue) and observational estimate (red). Thin green, pink, and black lines represent individual members of the CESM2-LENS, CAM6 AMIP, and piControl ensemble, respectively. Individual time series are smoothed using a 13-month running average.

experiment) primarily stems from the low correlation between the observed and simulated precipitation, which presumably reflects the role of internal atmospheric variability on year-to-year changes in precipitation.

To demonstrate that internal variability alone cannot explain the observed weakening of large-scale atmospheric circulations in recent decades, we analyze 34-year composites from the CMIP6 piControl runs (Figure 3 and Figure S7 in Supporting Information S1). The piControl ensemble is equally divided into strengthening and weakening trends, suggesting internal variability alone can result in either weakening or strengthening of the overturning circulation but cannot explain the magnitude of weakening observed in recent decades.

4. Conclusions and Discussion

In this work, we utilize satellite-based observations and the latest version of climate models to analyze trends in atmospheric overturning circulation during the satellite era. For all three indices used, we find a robust weakening

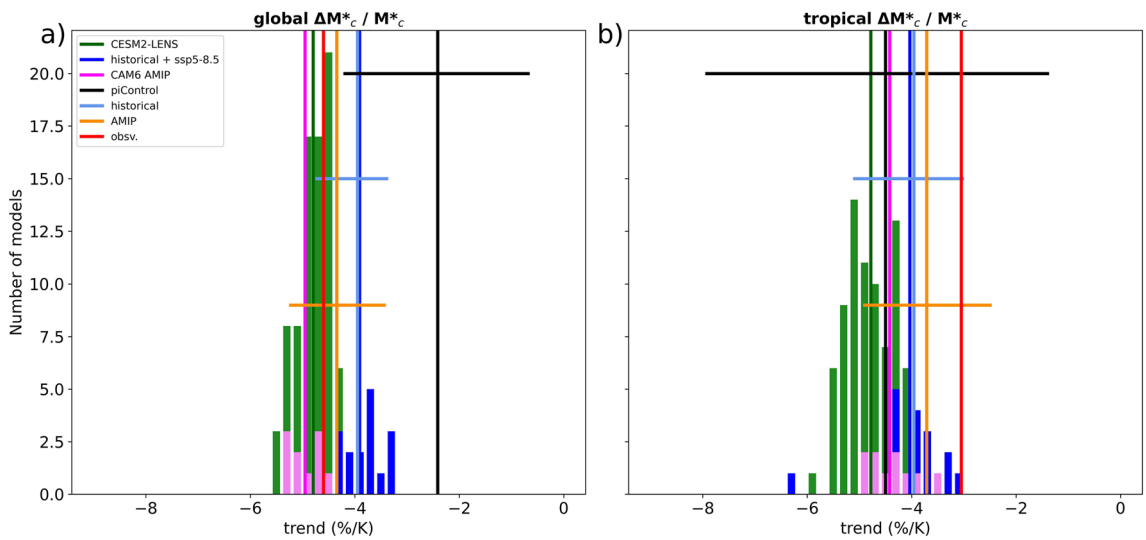

Figure 4. *Long-term trend in large-scale atmospheric circulation per K global warming*: Trend (1988–2021) in the fractional change in the convective mass flux for historical + ssp5-8.5 (blue), CESM2-LENS (green), CAM6 AMIP (pink), and piControl (black) experiments normalized by global-mean surface air temperature trend. The red line represents the observational estimate. Multi-model mean along with the ±2σ intermodel spread for AMIP and historical experiment (1979–2014) are represented by the orange and pale blue lines, respectively. Bin size = 0.2%/K.

of the atmospheric overturning circulation for both the AMIP and the coupled historical experiments. Further analysis of single-model large ensembles also shows a weakening of the atmospheric overturning circulation with warming. A comparable magnitude of global-mean overturning circulation weakening is seen in observations, within the range of CESM2-LENS, suggesting a role of anthropogenic forcing in the observed weakening in recent decades. In contrast, the piControl runs suggest that internal variability alone cannot explain the magnitude of the observed atmospheric overturning circulation weakening.

In both AMIP and the historical experiments, this weakening is dominated by a weakening of the zonally asymmetric component of the circulation. Despite having a similar thermodynamic response to global-mean surface warming for atmospheric overturning circulation, the AMIP and the coupled historical experiments show opposing trends in the regional-level Pacific WC. A recent study shows that the Pacific WC does weaken in accordance with the hydrologic constraint, but this effect is small compared to the effect of the recent SST pattern (Watanabe et al., 2023). This complex coupling between large-scale atmospheric circulation and regional-level circulations requires further analysis. Attempts to understand the mechanisms of WC weakening with warming have pointed at an inverse relation with gross moist stability, related to an increase in the vertical depth of deep convection (Duffy & O'Gorman, 2023; Wills et al., 2017).

Although the weakening of atmospheric overturning circulation is robust across climate models (except for the piControl experiments) and observations, individual models/ensemble members exhibit a large spread in the weakening per K global-mean warming. The weaker sensitivity of the observational estimate raises the question of models possibly overestimating the response to external forcing, especially in the case of CESM2-LENS.

Past works have shown contributions of fast response to radiative forcings, land-sea contrast and SST patterns on the hydrological cycle and consequently, regional circulation changes (Allan et al., 2020; Bony et al., 2013; He & Soden, 2015; Plesca et al., 2018). Our study shows a robust weakening of the atmospheric overturning circulation with global-mean surface warming, during the satellite era, independent of the SST warming pattern. However, questions remain about the coupling between large-scale atmospheric circulation and regional-level circulations and the influence of forcing biases within the models.

Data Availability Statement

CMIP6 (Eyring et al., 2016) data sets used in this study is available by a data archive developed and archived by the Earth System Grid Federation (ESGF). CMIP6 models used in this study are listed in Table S1 in Supporting Information S1. CESM2-LENS (Rodgers et al., 2021) data set is provided by the CESM2 Large Ensemble Community Project and supercomputing resources provided by the IBS Center for Climate Physics in South Korea. CAM6 (Danabasoglu et al., 2020) Prescribed Global SST AMIP Ensemble data set is provided by NCAR's Climate Variability and Change Working Group. GPCP (Adler et al., 2003) data is provided by NOAA PSL, Boulder, Colorado, USA. Merged Precipitable Water data is available at Remote Sensing Systems (2016). GISTEMPv4 data is provided by GISTEMP Team (2023). ERA5 data set is available at Hersbach et al. (2023).

Acknowledgments
This work was supported by NASA FINESST Grant 80NSSC21K1607 and NOAA Award NA21OAR4310351.

References

Adler, R. F., Huffman, G. J., Chang, A., Ferraro, R., Xie, P., Janowiak, J., et al. (2003). The version 2 global precipitation climatology project (GPCP) monthly precipitation analysis (1979-present). Journal of Hydrometeorology, *4*(6), 1147–1167. https://doi.org/10.1175/1525-7541(2003)004<1147:tvgpcp>2.0.co;2

Allan, R. P., Barlow, M., Byrne, M. P., Cherchi, A., Douville, H., Fowler, H. J., et al. (2020). Advances in understanding large-scale responses of the water cycle to climate change. *Annals of the New York Academy of Sciences*, *1472*(1), 49–75. https://doi.org/10.1111/nyas.14337

Allan, R. P., Willett, K. M., John, V. O., & Trent, T. (2022). Global changes in water vapor 1979–2020. *Journal of Geophysical Research: Atmospheres*, *127*(12), e2022JD036728. https://doi.org/10.1029/2022JD036728

Andrews, T., Bodas-Salcedo, A., Gregory, J. M., Dong, Y., Armour, K. C., Paynter, D., et al. (2022). On the effect of historical SST patterns on radiative feedback. *Journal of Geophysical Research: Atmospheres*, *127*(18), e2022JD036675. https://doi.org/10.1029/2022JD036675

Bellomo, K., & Clement, A. C. (2015). Evidence for weakening of the Walker Circulation from cloud observations. *Geophysical Research Letters*, *42*(18), 7758–7766. https://doi.org/10.1002/2015GL065463

Bony, S., Bellon, G., Klocke, D., Sherwood, S., Fermepin, S., & Denvil, S. (2013). Robust direct effect of carbon dioxide on tropical circulation and regional precipitation. *Nature Geoscience*, *6*, 447–451. https://doi.org/10.1038/ngeo1799

Bordbar, M. H., Martin, T., Latif, M., & Park, W. (2017). Role of internal variability in recent decadal to multidecadal tropical Pacific climate changes. *Geophysical Research Letters*, *44*(9), 4246–4255. https://doi.org/10.1002/2016GL072355

Chadwick, R., Boutle, I., & Martin, G. (2013). Spatial patterns of precipitation change in CMIP5: Why the rich do not get richervin the tropics. *Journal of Climate*, *26*(11), 3803–3822. https://doi.org/10.1175/JCLI-D-12-00543.1

Chung, E. S., Timmermann, A., Soden, B. J., Ha, K.-J., Shi, L., & John, V. O. (2019). Reconciling opposing Walker circulation trends in observations and model projections. *Nature Climate Change*, *9*(5), 405–412. https://doi.org/10.1038/s41558-019-0446-4

Danabasoglu, G., Lamarque, J.-F., Bacmeister, J., Bailey, D. A., DuVivier, A. K., Edwards, J., et al. (2020). The community earth System model version 2 (CESM2). Journal of Advances in Modeling Earth Systems, *12*, e2019MS001916. https://doi.org/10.1029/2019MS001916

DiNezio, P. N., Vecchi, G. A., & Clement, A. C. (2013). Detectability of changes in the Walker Circulation in response to global warming. *Journal of Climate*, *26*(12), 4038–4048. https://doi.org/10.1175/JCLI-D-12-00531.1

Duffy, M. L., & O'Gorman, P. A. (2023). Intermodel spread in Walker Circulation responses linked to spread in moist stability and radiation responses. *Journal of Geophysical Research: Atmospheres*, *128*(1), e2022JD037382. https://doi.org/10.1029/2022JD037382

England, M., McGregor, S., Spence, P., Meehl, G., Timmermann, A., Wenju, C., et al. (2014). Recent intensification of wind-driven circulation in the Pacific and the ongoing warming hiatus. *Nature Climate Change*, *4*(3), 222–227. https://doi.org/10.1038/nclimate2106

Eyring, V., Bony, S., Meehl, G. A., Senior, C. A., Stevens, B., Stouffer, R. J., & Taylor, K. E. (2016). Overview of the coupled model intercomparison project phase 6 (CMIP6) experimental design and organization. Geoscientific Model Development, *9*(5), 1937–1958. https://doi.org/10.5194/gmd-9-1937-2016

Falster, G., Konecky, B., Coats, S., & Stevenson, S. (2023). Forced changes in the Pacific Walker Circulation over the past millennium. *Nature*, *622*(7981), 93–100. https://doi.org/10.1038/s41586-023-06447-0

Gates, W. L., Boyle, J. S., Covey, C., & Dease, C. G. (1999). An overview of the results of the atmospheric mode intercomparison project (AMIP I). *Bulletin of the American Meteorological Society*, *80*(1), 29–56. https://doi.org/10.1175/1520-0477(1999)080<0029:AOOTRO>2.0.CO;2

GISTEMP Team. (2023). GISS surface temperature analysis (GISTEMP), version 4 [Dataset]. NASA Goddard Institute for Space Studies. Retrieved from https://data.giss.nasa.gov/gistemp/

He, J., & Soden, B. J. (2015). Anthropogenic weakening of the tropical circulation: The relative roles of direct CO_2 forcing and sea surface temperature change. *Journal of Climate*, *28*(22), 8728–8742. https://doi.org/10.1175/JCLI-D-15-0205.1

Held, I. M., & Soden, B. J. (2006). Robust responses of the hydrological cycle to global warming. *Journal of Climate*, *19*(21), 5686–5699. https://doi.org/10.1175/JCLI3990.1

Hersbach, H., Bell, B., Berrisford, P., Biavati, G., Horányi, A., Muñoz Sabater, J., et al. (2023). ERA5 monthly averaged data on single levels from 1940 to present [Dataset]. Copernicus Climate Change Service (C3S) Climate Data Store (CDS). https://doi.org/10.24381/cds.f17050d7

Knutson, T. R., & Manabe, S. (1995). Time-mean response over the tropical Pacific to increased CO_2 in a coupled ocean-atmosphere model. *Journal of Climate*, *8*(9), 2181–2199. https://doi.org/10.1175/1520-0442(1995)008<2181:TMROTT>2.0.CO;2

Kociuba, G., & Power, S. B. (2015). Inability of CMIP5 models to simulate recent strengthening of the Walker circulation: Implications for projections. *Journal of Climate*, *28*(1), 20–35. https://doi.org/10.1175/JCLI-D-13-00752.1

Lambert, F. H., & Webb, M. J. (2008). Dependency of global mean precipitation on surface temperature. *Geophysical Research Letters*, *35*(16), L16706. https://doi.org/10.1029/2008GL034838

Lau, W. K. M., & Kim, K. M. (2015). Robust Hadley Circulation changes and increasing global dryness due to CO_2 warming from CMIP5 model projections. *Proceedings of the National Academy of Sciences of the United States of America*, *112*(12), 3630–3635. https://doi.org/10.1073/pnas.1418682112

Lee, S., L'Heureux, M., Wittenberg, A. T., Seager, R., O'Gorman, P. A., & Johnson, N. C. (2022). On the future zonal contrasts of equatorial Pacific climate: Perspectives from observations, simulations, and theories. *npj Climate and Atmospheric Sciences*, *5*(1), 82. https://doi.org/10.1038/s41612-022-00301-2

Lenssen, N. J. L., Schmidt, G. A., Hansen, J. E., Menne, M. J., Persin, A., Ruedy, R., & Zyss, D. (2019). Improvements in the GISTEMP uncertainty model. *Journal of Geophysical Research: Atmospheres*, *124*(12), 6307–6326. https://doi.org/10.1029/2018JD029522

L'Heureux, M., Lee, S., & Lyon, B. (2013). Recent multidecadal strengthening of the Walker Circulation across the tropical Pacific. *Nature Climate Change*, *3*(6), 571–576. https://doi.org/10.1038/nclimate1840

Loeb, N. G., Wang, H., Allan, R., Andrews, T., Armour, K., Cole, J. N. S., et al. (2020). New generation of climate models track recent unprecedented changes in Earth's radiation budget observed by CERES. *Geophysical Research Letters*, *47*(5), e2019GL086705. https://doi.org/10.1029/2019GL086705

Ma, J., Xie, S.-P., & Kosaska, Y. (2012). Mechanisms for tropical tropospheric circulation change in response to global warming. *Journal of Climate*, *25*(8), 2979–2994. https://doi.org/10.1175/JCLI-D-11-00048.1

McGregor, S., Timmermann, A., Stuecker, M. F., England, M. H., Merrifield, M., Jin, F.-F., & Chikamoto, Y. (2014). Recent Walker Circulation strengthening and Pacific cooling amplified by Atlantic warming. *Nature Climate Change*, *4*(10), 888–892. https://doi.org/10.1038/nclimate2330

Meng, Q., Latif, M., Park, W., Keenlyside, N. S., Semenov, V. A., & Martin, T. (2012). Twentieth century Walker Circulation change: Data analysis and model experiments. *Climate Dynamics*, *38*(9–10), 1757–1773. https://doi.org/10.1007/s00382-011-1047-8

Murphy, L. N., Bellomo, K., Cane, M., & Clement, A. (2017). The role of historical forcings in simulating the observed Atlantic multidecadal oscillation. *Geophysical Research Letters*, *44*(5), 2472–2480. https://doi.org/10.1002/2016GL071337

O'Gorman, P. A., & Singh, M. S. (2013). Vertical structure of warming consistent with an upward shift in the middle and upper troposphere. *Geophysical Research Letters*, *40*(9), 1838–1842. https://doi.org/10.1002/grl.50328

O'Neill, B. C., Tebaldi, C., van Vuuren, D. P., Eyring, V., Friedlingstein, P., Hurtt, G., et al. (2016). The scenario model intercomparison project (ScenarioMIP) for CMIP6. *Geoscientific Model Development*, *9*, 3461–3482. https://doi.org/10.5194/gmd-9-3461-2016

Plesca, E., Buehler, S. A., & Grützun, V. (2018). The fast response of the tropical circulation to CO_2 forcing. *Journal of Climate*, *31*(24), 9903–9920. https://doi.org/10.1175/JCLI-D-18-0086.1

Power, S. B., & Kociuba, G. (2011). What caused the observed twentieth-century weakening of the Walker circulation? *Journal of Climate*, *24*(24), 6501–6514. https://doi.org/10.1175/2011JCLI4101.1

Power, S. B., Lengaigne, M., Capotondi, A., Khodri, M., Vialard, J., Jebri, B., et al. (2021). Decadal climate variability in the tropical Pacific: Characteristics, causes, predictability, and prospects. *Science*, *374*(6563), eaay9165. https://doi.org/10.1126/science.aay9165

Power, S. B., & Smith, I. N. (2007). Weakening of the Walker Circulation and apparent dominance of El Niño both reach record levels, but has ENSO really changed? *Geophysical Research Letters*, *34*(18), L18702. https://doi.org/10.1029/2007GL030854

Remote Sensing Systems. (2016). Monthly mean total precipitable water data set on a 1-degree grid made from Remote sensing Systems version-7 microwave radiometer data, V07r01 [Dataset]. Stl. Retrieved from https://www.remss.com/measurements/atmospheric-water-vapor/tpw-1-deg-product/

Rodgers, K. B., Lee, S.-S., Rosenbloom, N., Timmermann, A., Danabasoglu, G., Deser, C., et al. (2021). Ubiquity of human-induced changes in climate variability. Earth System Dynamics, *12*(4), 1393–1411. https://doi.org/10.5194/esd-12-1393-2021

Sandeep, S., Stordal, F., Sardeshmukh, P. D., & Compo, G. P. (2014). Pacific Walker Circulation variability in coupled and uncoupled climate models. *Climate Dynamics*, *43*(1–2), 103–117. https://doi.org/10.1007/s00382-014-2135-3

Seager, R., Henderson, N., & Cane, M. (2022). Persistent discrepancies between observed and modeled trends in the tropical Pacific Ocean. *Journal of Climate*, *35*(14), 4571–4584. https://doi.org/10.1175/JCLI-D-21-0648.1

Sherwood, S. C., Bony, S., & Dufresne, J.-L. (2014). Spread in model climate sensitivity traced to atmospheric convective mixing. *Nature*, *505*(7481), 37–42. https://doi.org/10.1038/nature12829

Sohn, B. J., & Park, S. C. (2010). Strengthened tropical circulations in past three decades inferred from water vapor transport. *Journal of Geophysical Research*, *115*(D15), D15112. https://doi.org/10.1029/2009JD013713

Sohn, B. J., Yeh, S. W., Schmetz, J., & Song, H.-J. (2013). Observational evidences of Walker Circulation change over the last 30 years contrasting with GCM results. *Climate Dynamics*, *40*(7–8), 1721–1732. https://doi.org/10.1007/s00382-012-1484-z

Su, H., Jiang, J. H., Zhai, C., Shen, T. J., Neelin, D., Stephens, G. L., & Yung, Y. L. (2014). Weakening and strengthening structures in the Hadley Circulation change under global warming and implications for cloud response and climate sensitivity. *Journal of Geophysical Research: Atmospheres*, *119*(10), 5787–5805. https://doi.org/10.1002/2014JD021642

Su, H., Zhai, C., Jiang, J. H., Wu, L., Neelin, J. D., & Yung, Y. L. (2019). A dichotomy between model responses of tropical ascent and descent to surface warming. *npj Climate and Atmospheric Science*, *2*(8), 8. https://doi.org/10.1038/s41612-019-0066-8

Tokinaga, H., Xie, S. P., Deser, C., Kosaka, Y., & Okumura, Y. M. (2012). Slowdown of the Walker Circulation driven by tropical Indo-Pacific warming. *Nature*, *491*(7424), 439–443. https://doi.org/10.1038/nature11576

Vecchi, G. A., & Soden, B. J. (2007). Global warming and the weakening of the tropical circulation. *Journal of Climate*, *20*(17), 4316–4340. https://doi.org/10.1175/JCLI4258.1

Vecchi, G. A., Soden, B. J., Wittenberg, A. T., Held, I. M., Leetmaa, A., & Harrison, M. J. (2006). Weakening of tropical Pacific atmospheric circulation due to anthropogenic forcing. *Nature*, *441*(7089), 73–76. https://doi.org/10.1038/nature04744

Watanabe, M., Dufresne, J.-L., Kosaka, Y., Mauritsen, T., & Tatebe, H. (2021). Enhanced warming constrained by past trends in equatorial Pacific sea surface temperature gradient. *Nature Climate Change*, *11*(1), 33–37. https://doi.org/10.1038/s41558-020-00933-3

Watanabe, M., Iwakiri, T., Dong, Y., & Kang, S. M. (2023). Two competing drivers of the recent Walker circulation trend. *Geophysical Research Letters*, *50*, e2023GL105332. https://doi.org/10.1029/2023GL105332

Weatherhead, E. C., Reinsel, G. C., Tiao, G. C., Meng, X.-L., Choi, D., Cheang, W.-K., et al. (1998). Factors affecting the detection of trends: Statistical considerations and applications to environmental data. *Journal of Geophysical Research*, *103*(D14), 17149–17161. https://doi.org/10.1029/98JD00995

Wills, R. C. J., Dong, Y., Proistosecu, C., Armour, K. C., & Battisti, D. S. (2022). Systematic climate model biases in the large-scale patterns of recent sea-surface temperature and sea-level pressure change. *Geophysical Research Letters*, *49*(17), e2022GL100011. https://doi.org/10.1029/2022GL100011

Wills, R. C. J., Levine, X. J., & Schneider, T. (2017). Local energetic constraints on Walker Circulation strength. *Journal of the Atmospheric Sciences*, *74*(6), 1907–1922. https://doi.org/10.1175/JAS-D-16-0219.1

Wodzicki, K. R., & Rapp, A. D. (2020). Variations in precipitating convective feature populations with ITCZ width in the Pacific Ocean. *Journal of Climate*, *33*(10), 4391–4401. https://doi.org/10.1175/JCLI-D-19-0689.1

Wu, M., Zhou, T., Li, C., Li, H., Chen, X., Wu, B., et al. (2021). A very likely weakening of Pacific Walker Circulation in constrained near-future projections. *Nature Communications*, *12*(1), 6502. https://doi.org/10.1038/s41467-021-26693-y